Analytical Methods

ROYAL SOCIETY OF CHEMISTRY

TUTORIAL REVIEW

View Article Online
View Journal

Cite this: DOI: 10.1039/d1ay00588j

Taylor dispersion analysis in fused silica capillaries: a tutorial review

Meagan R. Moser [ab] and Christopher A. Baker [*b]

Biological and pharmaceutical analytes like liposomes, therapeutic proteins, nanoparticles, and drug-delivery systems are utilized in applications, such as pharmaceutical formulations or biomimetic models, in which controlling their size is often critical. Many of the common techniques for sizing these analytes require method development, significant sample preparation, large sample quantities, and lengthy analysis times. In other cases, such as DLS, sizing can be biased towards the largest constituents in a mixture. Therefore, there is a need for more rapid, sensitive, accurate, and straightforward analytical methods for sizing macromolecules, especially those of biological origin which may be sample-limited. Taylor dispersion analysis (TDA) is a sizing technique that requires no calibration and consumes only nL to pL sample volumes. In TDA, average diffusion coefficients are determined *via* the Taylor–Aris equation by characterizing band broadening of an analyte plug under well-controlled laminar flow conditions. Diffusion coefficient can then be interpreted as hydrodynamic radius (R_H) *via* the Stokes–Einstein equation. Here, we offer a tutorial review of TDA, intended to make the method better understood and more widely accessible to a community of analytical chemists and separations scientists who may benefit from the unique advantages of this versatile sizing method. We first provide a tutorial on the fundamental principles that allow TDA to achieve calibration-free sizing of analytes across a wide range of R_H, with an emphasis on the reduced sample consumption and analysis times that result from utilizing fused silica capillaries. We continue by highlighting relationships between operating parameters and critically important flow conditions. Our discussion continues by looking at methods for applying TDA to sample mixtures *via* algorithmic approaches and integration of capillary electrophoresis and TDA. Finally, we present a selection of reports that demonstrate TDA applied to complex challenges in bioanalysis and materials science.

Received 6th April 2021
Accepted 6th May 2021

DOI: 10.1039/d1ay00588j

rsc.li/methods

[a]*Department of Chemistry, University of Tennessee, Knoxville, Tennessee, 37996, USA*

[b]*Department of Chemistry and Biochemistry, New Mexico State University, MSC 3C, PO Box 30001, Las Cruces, New Mexico, 88003, USA. E-mail: cabaker@nmsu.edu; Tel: +1-575-646-1015*

Meagan R. Moser completed her BS in Chemistry at The University of Tennessee, Knoxville in 2016, where she is currently a fifth-year graduate student pursuing a PhD in Analytical Chemistry. Her research involves the development of analytical tools for the characterization of biological macromolecules by Taylor dispersion analysis.

Christopher A. Baker earned his BS in Chemistry from Wayne State University in 2007, and his PhD in Bioanalytical Chemistry from Florida State University in 2012. He was a postdoctoral associate at The University of Arizona (2012–2014), and Sandia National Laboratories (2014–2015), and an assistant professor of chemistry at the University of Tennessee (2015–2020). He is currently an assistant professor in the Department of Chemistry & Biochemistry at New Mexico State University. The Baker Bioanalysis Lab leverages expertise in separation science and micro- and nanofabrication to develop new technologies for studying neurochemistry and astrobiology.

Introduction

Designing and producing drug delivery systems, therapeutic proteins, nanoparticles, and biopolymers requires fast and straightforward characterization of these products *via* high accuracy and high sensitivity analytical methods. Many standard methods for solution-phase size characterization require extensive method development, tedious sample preparation, large sample volumes, lengthy analysis times, and/or expensive instrumentation. One widely used size characterization method is dynamic light scattering (DLS), which can, in some cases, be performed with limited sample preparation and offer rapid analysis times. Complex samples such as blood plasma have been analyzed by DLS with preparation as simple as dilution, filtration and/or centrifugation.[1,2] However, signal intensity in DLS is proportional to the analyte radius raised to the 6^{th} power,[3] which makes detection sensitivity particularly challenging when characterizing small particles. For the same reason, DLS is sensitive to issues of analyte aggregation.[3] These qualities are often disadvantageous when interrogating the size of small proteins, especially in the presence of larger proteins or aggregates. Hawe *et al.* measured a range of concentrations (0.05–50 mg mL^{-1}) of various peptides and proteins.[4] While DLS accurately sized the antibody drug adalimumab (5–6 nm) at the lowest concentration, sizing the peptide oxytocin (~0.8 nm) was not possible at low concentrations due to the influence of dust or excipients in the sample. In this case, DLS provided inaccurate and inconsistent hydrodynamic radius (R_H) determinations for oxytocin ranging from 6.9–130 nm. In the same work, DLS was utilized to observe aggregation in heat-stressed formulations of protein samples. With a 5 °C increase in temperature, a model IgG antibody showed an increase from $R_H = 7.5$ nm to $R_H = 22$ nm by DLS, whereas TDA measured a modest increase from $R_H = 6.5$ nm to $R_H = 7.5$ nm under identical conditions. This disagreement was attributed to the bias of DLS towards large particles, in which the largest particles or aggregates dominate the overall scattering intensity, thus resulting in inaccurately high R_H determinations.

Size exclusion chromatography (SEC) is another method often employed for size determination. SEC requires precise calibration with appropriate size standards, and is susceptible to deleterious effects of analyte–column interactions.[5] Pacáková *et al.* found that melittin, a strongly basic peptide found in bee venom, displayed deleterious retention on a hydrophilic SEC column, which they attributed to the peptide's inability to form a predominantly hydrophilic shell due to the uneven distribution of exterior hydrophilic residues.[6] Overcoming these deleterious analyte–column interactions required method optimization such as the addition of an organic solvent to the mobile phase and pH optimization. Ricker *et al.* explain that SEC columns can exhibit electrostatic effects when the mobile phase ionic strength is low, and hydrophobic effects when ionic strength is high.[7] Either case can result in deleterious retention of analytes, which can result in peak deformation and, ultimately, inaccuracy of size determinations by SEC. They observed the effect of mobile phase ionic strength on SEC of three mouse myeloma antibodies using a silica-based stationary phase material. At low ionic strength, the least basic antibody had no net positive charge, and was therefore unaffected by adsorption to the anionic silanols at the stationary phase surface. However, at high ionic strength, the antibody was retained due to hydrophobic effects. This work demonstrates the careful consideration for method development that is needed for accurate size determinations by SEC.

Various micro- and nanoscopic imaging techniques such as transmission electron microscopy (TEM), scanning electron microscopy, and atomic force microscopy have been applied to particle sizing.[8–14] However, field of view ultimately limits the throughput of analysis for any imaging technique applied to molecular or particle sizing.

Taylor dispersion analysis (TDA) is a powerful analytical method for size characterization that addresses many of the shortcomings of the more common methods described above. Size determinations by TDA are absolute, requiring no calibration nor prior knowledge of sample concentration.[15] TDA conducted in fused silica capillaries requires only sub-nanoliter sample volumes, and the method can be applied to sizing analytes from small molecules[16–20] to micron-scale particles and complexes.[21,22] TDA has evolved from studying gaseous diffusion coefficients in large tubes[23–25] to TDA measurements of therapeutic proteins,[26–36] drug delivery systems,[26,30,37–42] nanoparticles,[43–52] mixtures,[15,44,53–59] synthetic polymers,[30,60–64] and more. While TDA has been discussed in other reviews of physiochemical characterization methods in specific application areas,[65–70] to our knowledge no recent review has combined a tutorial discussion of the underlying principles and practical considerations of TDA with an outline of the breadth and depth of modern TDA applications. Here, we offer a tutorial review of TDA, intended to make the method better understood and more widely accessible to a community of analytical chemists and separations scientists who may benefit from the unique advantages of this versatile sizing method.

Principles of TDA

First described by Taylor in 1953,[23] TDA enables the direct determination of diffusion coefficients across a wide range of hydrodynamic radii (Å to μm). TDA is a mathematical framework for analyzing dispersion that results from the interaction between the parabolic velocity profile of pressure driven laminar flow in a cylindrical tube and the radial diffusion of analytes across that velocity profile. A sample plug injected into flow spreads axially due to the combined effects of convection and diffusion, which is observed as band broadening (Fig. 1). Diffusion occurs both radially and longitudinally, however TDA is conducted under well-controlled flow conditions (discussed in more detail below) that ensure the contribution to band broadening from longitudinal diffusion is negligible. As a result of the parabolic velocity profile, the initial velocity of any individual analyte molecule or particle is a function of its starting radial position within the injected sample plug. As radial diffusion proceeds, each molecule or particle samples the full range of flow velocities in the parabolic profile over the duration

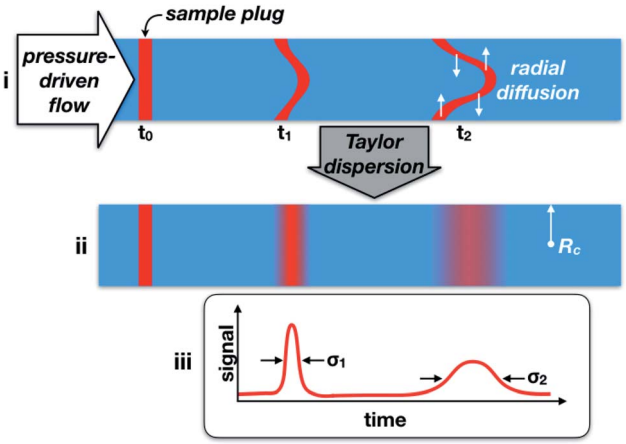

Fig. 1 Illustration of Taylor dispersion, and the corresponding variables utilized in TDA. Under the parabolic velocity profile of pressure-driven flow, and neglecting any effects of diffusion, a sample plug would deform as illustrated (i). Considering the effects of diffusion only in the radial direction gives Taylor dispersion, yielding the band profiles illustrated (ii). The evolution of Taylor dispersion can be observed as band broadening of a peak measured at multiple locations in the flow path (iii). The variables t_1, t_2, R_c, σ_1, and σ_2 are the same variables utilized in eqn (13).

of flow, resulting in an ensemble average velocity across all particles in the sample population.

Analytes with low diffusion coefficients move slowly across the parabolic velocity profile such that two analyte particles starting with disparate velocities remain separated within their respective flow streams for a longer duration as compared to the behavior of analytes with higher diffusion coefficients. The net result is a broad distribution of velocities about the population mean velocity for analytes with low diffusion coefficients, which is observed as a high degree of band broadening. Conversely, molecules with relatively high diffusion coefficients move rapidly across the parabolic velocity profile, experiencing a narrower distribution of velocities about the population mean, thus a lower degree of band broadening is observed.

It is worth noting here that the relationship between diffusion coefficient and band broadening observed by TDA may seem counterintuitive to many separations scientists more accustomed to considering longitudinal diffusion. By the mechanism of longitudinal diffusion, higher rates of diffusion result in increased band broadening, which is the opposite of what is described above. Nevertheless, when considering only radial diffusion in TDA measurements, molecular diffusion coefficients (D) can be determined by observing the degree of band broadening as follows:[71,72]

$$D = \frac{R_c^2 t_d}{24\sigma^2} \quad (1)$$

where R_c is the channel radius, t_d is the average elution time, and σ^2 is the peak variance. D can be used as a structural descriptor of the analyte when transformed to R_H *via* the Stokes–Einstein relation:[73]

$$R_H = \frac{k_B T}{6\pi\eta D} \quad (2)$$

where k_B is the Boltzmann constant, T is temperature, and η is the dynamic viscosity of the solution.

For TDA to yield accurate determinations of D, precise control of flow is required to meet two requisite conditions known as the Taylor conditions. First, TDA considers radial diffusion while neglecting longitudinal diffusion. For this to be possible, the rate of advection must be significantly greater than the rate of diffusion, which is widely considered to be satisfied when the Péclet number (Pe) is greater than 69.[74] Pe is defined for a cylindrical channel as:[72]

$$\mathrm{Pe} = \frac{uR_c}{D} \quad (3)$$

where u is the linear flow rate. In his original work,[74] Taylor defined the following inequality as a requirement to satisfy eqn (1):

$$\frac{4L}{R_c} \gg \frac{uR_c}{D} \gg 6.9 \quad (4)$$

where L is the length of the channel. In that work, a ratio of 1 : 10 between the inequalities was considered requisite, which gives the accepted Taylor condition Pe $\geq$ 69. Cottet *et al.* demonstrated that longitudinal diffusion can be neglected even in conditions where Pe < 69, defining requisite flow velocity as:[56]

$$u \geq \frac{D}{R_c}\sqrt{\frac{48}{\varepsilon}} \quad (5)$$

where ε is the relative error in determination of D. By this analysis, Taylor's condition of Pe $\geq$ 69 gives a relative error due to neglecting longitudinal diffusion of 1%, whereas Cottet and coworkers suggest that a relative error of 3% can be tolerated, leading to the requisite condition Pe $\geq$ 40.

The second Taylor condition describes the duration for which a sample plug must remain in flow in order to observe sufficient band-broadening effects due to Taylor dispersion. Taylor's original work described the condition as follows: "the time necessary for appreciable effects to appear, owing to convective transport [must be] long compared with the 'time of decay' during which radial variations of concentration are reduced to a fraction of their initial value through the action of molecular diffusion".[23] As such, the requisite residence time (t_R) of the sample plug in flow is influenced by D and R_c. Residence time can be normalized for these factors to give a dimensionless time factor (τ) defined as:

$$\tau = \frac{Dt_R}{R_c^2} \quad (6)$$

Taylor expresses eqn (6) as the inequality[74]

$$D \gg \frac{R_c^2}{4t_R} \quad (7)$$

Taking a 1 : 10 ratio as satisfying inequality (7), the following condition satisfies minimum required t_R:

$$t_R \geq 2.5\frac{{R_c}^2}{D} \quad (8)$$

Substituting t_R in eqn (6) with inequality (8), we can obtain the minimum required value for τ:

$$\tau = \frac{Dt_R}{{R_c}^2} = \frac{D\left(2.5\frac{{R_c}^2}{D}\right)}{{R_c}^2} \geq 2.5 \quad (9)$$

Alternative minimum τ values have also been reported. In the same work that studied alternative minimum Pe conditions, Cottet *et al.* demonstrate that the minimum t_R can also be expressed as a function of ε as follows[56]

$$t_R \geq \frac{3{R_c}^2}{80D\varepsilon} \quad (10)$$

Presuming an acceptable ε of 3%, inequality (10) becomes:

$$t_R \geq \frac{1.25{R_c}^2}{D} \quad (11)$$

Substituting t_R in eqn (6) with inequality (11), we can obtain the minimum required value for τ:

$$\tau = \frac{Dt_R}{{R_c}^2} = \frac{D\left(1.25\frac{{R_c}^2}{D}\right)}{{R_c}^2} \geq 1.25 \quad (12)$$

There is some disagreement on appropriate limiting value of τ. Several works report the condition $\tau > 1.4$.[45,72,75,76] However, to our knowledge, no mathematical basis for alternate limiting τ values has been offered with the rigor of either Taylor or Cottet's solutions shown above.

Practical considerations for TDA measurements

Several practical considerations arise from the requisite Taylor conditions. First, eqn (6) shows that analysis times can be dramatically reduced by reducing R_c. This has motivated the use of fused silica capillaries (typ. 10–250 μm i.d.) as flow systems for TDA. As a result, capillary electrophoresis (CE) instrumentation has become a prominent tool in the continued development and application of TDA. Second, although TDA is a method for determining D, target values of D are needed to define the requisite Taylor conditions. Since the Taylor conditions are met by exceeding thresholds (*i.e.* $\tau \geq 2.5$ and Pe ≥ 69), *a priori* knowledge of D is not required. Instead, careful consideration is needed to bracket an appropriate range of D values for a given analysis, which can be used to deduce the limiting values of operating parameters u, R_c, and t_R that satisfy the Taylor conditions. Finally, it is impractical to consider the two requisite Taylor conditions independently when designing the parameters of a TDA experiment. For example, Pe must exceed a value of 69 but is given no theoretical upper bound, which suggests there is no upper bound of the operating parameter u and therefore flow velocity should be maximized. While u is not given an upper bound on the basis of theory, increasing u requires increasing capillary length in order to achieve a value for t_R to satisfy $\tau > 2.5$, and impractical capillary lengths can quickly arise from poorly chosen u values. Thus, practical limitations require a careful selection of operating parameters to meet the Taylor conditions for an appropriately bracketed range of D. With careful consideration, and several iterative calculations of eqn (3) and (6), selecting appropriate and practical operating conditions for TDA is not prohibitively laborious. Still, making available purpose-built calculation tools for establishing appropriate operating parameters would benefit researchers currently utilizing TDA and may foster more widespread adoption of the technique.

Practical and theoretical limitations exist beyond the scope of appropriately selecting operating parameters to meet the requisite Taylor conditions. For example, the TDA principles described above assume that the sample plug remains under continuous flow for the full duration of t_R. In practice, this can be difficult or impossible to achieve, especially when utilizing CE instrumentation. The act of injecting a sample plug *via* conventional CE injection methods necessarily gives discontinuous flow velocities because flow must be stopped to bring a sample vial to the capillary inlet and stopped again to return a buffer vial to the capillary inlet before flow recommences for the TDA procedure. A key to overcoming this limitation has been the use of dual-detector schemes,[16,17,77,78] in which band broadening is compared between two detection points positioned on the flow path to achieve the appropriate t_R value within the volume between the detection points. In this way, band broadening evolves while under continuous flow between the two detection points, and any contribution to overall band broadening from discontinuous flow in the sample injection process is accounted for in the initial observation at the first detection point. Dual-detector TDA utilizes a modified form of the Taylor–Aris equation as follows:[76]

$$D = \frac{{R_c}^2(t_2 - t_1)}{24({\sigma_2}^2 - {\sigma_1}^2)} \quad (13)$$

where t_1 and t_2 are the peak arrival times at detectors 1 and 2, respectively, and ${\sigma_1}^2$ and ${\sigma_2}^2$ are the peak variances as observed at detectors 1 and 2, respectively.

Chamieh *et al.* compared the performance of TDA in single- and dual-point detection configurations.[53] In their work, TDA of monodisperse albumin proteins and polydisperse polymer standard samples was performed utilizing a commercial CE instrument equipped with a 60 cm × 50 μm i.d. fused silica capillary and UV absorbance detector. For single-point detection, band broadening was analyzed for signals collected at three detector positions (effective capillary lengths: 8.5 cm, 24.5 cm, and 51.5 cm). For dual-point detection, signals were analyzed with detection points positioned at 24.5 cm and 51.5 cm. Unsurprisingly, single-point detection TDA resulted in overestimates of R_H when the injection volume was a significant fraction (>1%) of the total effective capillary volume. Utilizing

previously reported mathematical corrections[17] for the effects of pressure ramping and the finite volume of the injection plug, R_H determinations by single-point detection TDA were not statistically different from those determined by dual-point detection, provided injection volume remained <1% of effective capillary volume. However, dual-point detection TDA is arguably preferable, as it does not require any mathematical corrections or presumptions of dynamic flow conditions which may be difficult to observe. To facilitate precision TDA, technologies have been developed to achieve dual-detector configurations in commercial CE instrumentation for UV absorbance[17] and fluorescence detection[16] modes.

TDA analysis times are significantly reduced by decreasing R_c, which has motivated the use of fused silica capillaries. Precise control of applied pressures to a capillary flow system can be achieved with modern commercial CE instrumentation, making these instruments well suited for TDA. Williams and Vigh leveraged the integration of CE and TDA in a commercial instrument by first separating analytes by CE then switching to pressure driven flow to perform TDA on the separated analytes.[79] One critical challenge to performing TDA in a commercial CE instrument was described by Sharma *et al.*, who described the effects of the initial ramp in flow velocity that occurs upon pressure application.[72] This non-uniform velocity profile introduces significant error in determinations of D. To circumvent this effect, ramp rate can be characterized and corrected for mathematically. The ramp rate of the CE instrument must be determined and used to convert the observed residence time to the ideal residence time by the equation:

$$t_R = \frac{t_{R,obs} + \sqrt{{t_{R,obs}}^2 - 16 L_T L_D \eta / {R_c}^2 r_i}}{2} \quad (14)$$

where L_T is capillary length, L_D is tube length from inlet to detector, and r_i is the rate of increase of applied pressure. When there is no initial velocity ramp, $t_R = t_{R,obs}$ and D can be determined simply by eqn (1). However, a velocity ramp leads to errors in the measured values of D if not corrected using eqn (14). With increased $t_{R,obs}$ the effect of r_i becomes negligible, and as $t_{R,obs}$ approaches infinity, any error in D would approach zero. Thus, the effect of the ramp is greater at lower $t_{R,obs}$. To demonstrate this, the error in D determinations for phenylalanine was characterized as a function of $t_{R,obs}$. Errors greater than 50% were observed for $t_{R,obs}$ < 50 s whereas <1% error was observed for $t_{R,obs}$ > 100 s. Correcting for flow velocity ramp by eqn (14), reduced the error at all $t_{R,obs}$ evaluated to <2%. While this correction was straightforward for frontal analysis, zonal analysis required additional corrections to account for the finite width of the injection plug. The additional correction required the calibration of observed peak variance (${\sigma_{obs}}^2$) *vs.* injection volume (V_i) at each t_R. Thus, correcting for a velocity ramp in zonal analysis can add substantial additional work to the overall workflow.

The operating principles of TDA are conceptually similar to those of hydrodynamic chromatography (HDC), although these are mechanistically distinct modes of analysis. Cottet and coworkers characterized the relationship between R_H, applied pressure, and capillary diameter to elucidate the conditions under which HDC mechanisms interfere with the accurate interpretation of TDA results.[80] In Fig. 2A and B, the red lines correspond to experimental conditions of constant analyte size (vertical line) or constant mobilizing pressure (horizontal lines), and the dots represent the conditions illustrated in Fig. 2C and D. When 250 nm polystyrene nanoparticles (PS NPs) were analyzed by TDA utilizing a 50 μm i.d. fused silica capillary under mobilization pressures from 7–550 mbar, peak shape became distorted at and above 90 mbar (Fig. 2C). Interestingly, the conditions with observed peak distortion corresponded to $\tau \leq 1.25$, which fails to satisfy the requisite Taylor condition. When various sizes of PS NPs (R_H = 110 nm, 250 nm, 500 nm) were analyzed by TDA utilizing 25 μm i.d. fused silica capillary and a fixed mobilizing pressure of 28 mbar, the effects of HDC reduced elution times of 250 nm and 500 nm PS NPs (Fig. 2D). Importantly, HDC affected the variance of the NP peaks even without appreciable effects on mean elution time, which adversely affected the accuracy in determinations of D. The authors identified an upper limit on the ratio of R_H to capillary radius (R_c) as a function of ε given by:

$$\frac{R_H}{R_c} = 0.17\varepsilon \quad (15)$$

In many cases, especially when designing TDA experiments for the analysis of macromolecular constructs, this constraint will warrant careful consideration when selecting appropriate operating parameters to meet the Taylor conditions.

Another important consideration is the potential for analyte-capillary adsorption, which will introduce peak asymmetry in the resulting elution profile, or taylorgram. Latunde-Dada *et al.* observed asymmetric peaks with pronounced tailing in varying concentrations of lysozyme (1–20 mg mL^{-1}) in a standard 75 μm i.d. capillary.[81] As an attempt to mitigate the effect of peak tailing on R_H determinations, they developed a constrained fitting algorithm to isolate dispersive components of the concentration profiles from the solute-capillary interacting components. This mathematical correction yielded improved accuracy in R_H determinations for high concentration (*i.e.* 5–20 mg mL^{-1}) lysozyme samples. Interestingly, at 1 mg mL^{-1} lysozyme, both free and constrained fits gave inaccurate R_H determinations (4.5 ± 0.3 nm and 3.33 ± 0.03 nm, for free and constrained fits, respectively as compared to previously reported values of 1.89–2.05 nm (ref. 82 and 83)). The authors postulated that these inaccuracies resulted from a much greater fraction of total sample engaged in adsorptive interactions at the capillary wall and, thus, subject to a net flow velocity that did not meet the Taylor criteria. Here, we suggest that adverse adsorption effects may warrant adapting common practices from CE methods, such as capillary surface modification or buffer additives,[61,84,85] for use in TDA measurements. Such efforts will require careful consideration and characterization of the effects on solution viscosity to yield accurate calibration-free size determinations.

Though the principles of TDA were first described in the early 1950s, modern capillary flow systems have enabled this

technology to be leveraged more recently as a powerful technique for size determination in various application areas and across various modes of analysis. For example, in addition to UV absorbance[17] and fluorescence detection[16,86] modes, TDA has been coupled to mass spectrometry,[87,88] refractive index detection,[62] and backscattering interferometry.[89] To this point, we have considered TDA of pure substances. TDA leverages tools common to separation science, and therefore it is interesting to examine how the practice and principles of TDA become more complex in the context of sample mixtures.

Algorithmic approaches to TDA of mixtures

TDA is applicable to both monodisperse and polydisperse samples.[53,55] For monodisperse samples, TDA results for the determination of R_H are directly analogous to those of DLS, which is a standard method for particle size characterization.[55] Conventionally, TDA gives weight-averaged or number averaged R_H values when utilizing mass- or concentration-sensitive detection modes, respectively.[15] Thus, the resulting R_H determinations for polydisperse samples can differ from the harmonic z-averaged R_H value obtained by DLS.[90] This incongruency with DLS has motivated various regression and statistical analysis approaches to improve the performance of TDA for mixtures and polydisperse samples.

Common peak fitting methods for non-Gaussian peak shapes have been applied to TDA data for the analysis of polydisperse samples. Deviations from a strict Gaussian peak shape were observed at the apex and base of taylorgrams produced from a mixture of third and fifth generation dendrigraft poly-L-lysine, complicating the determination of appropriate peak variance in the taylorgram.[53] In the case where Gaussian fits cannot be applied to taylorgrams of polydisperse samples, peak variance can be determined *via* an integration-based algorithm. In that work, peak variance was determined by integrating the whole signal of the resulting non-Gaussian peaks across the time interval using the following equation:

$$\sigma^2 = \frac{\int h(t)(t - t_d)^2 dt}{\int h(t) dt} = \frac{\sum_{m}^{i=n} h_i (t_i - t_d)^2 (t_{i+1} - t_i)}{\sum_{m}^{i=n} h_i (t_{i+1} - t_i)} \quad (16)$$

where $h(t)$ is detector response, t_i is elution time for a given point i, t_d is the average elution time, n and m are the starting and ending points considered for the integration. This

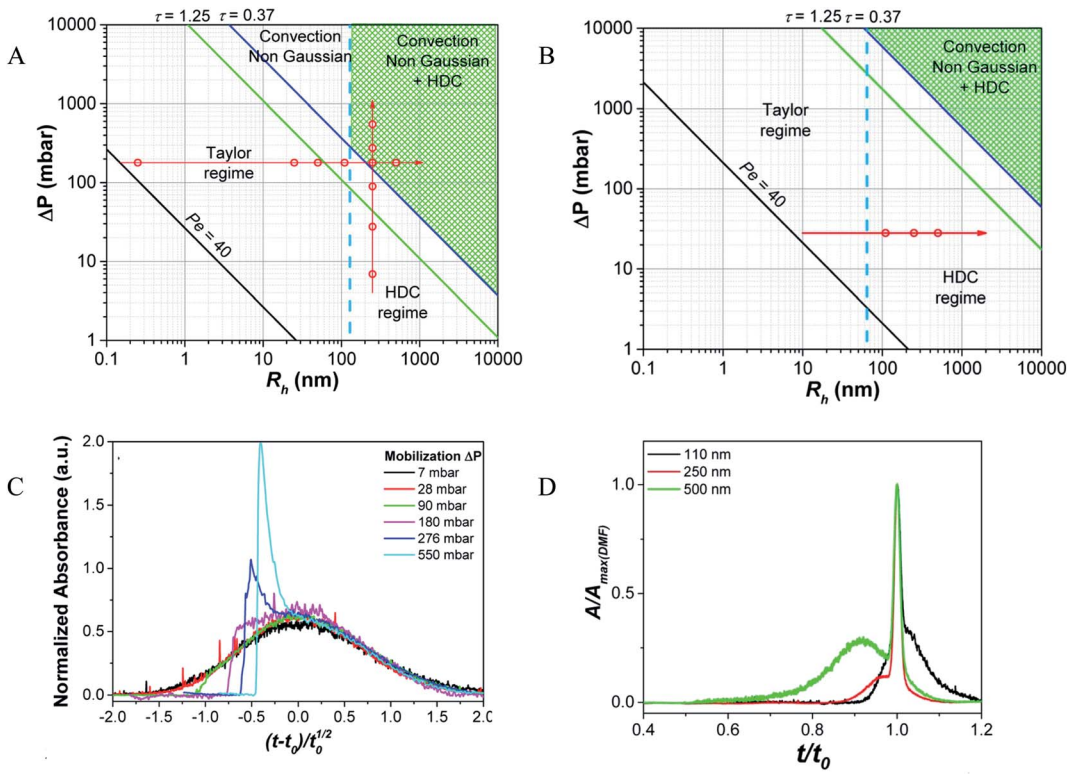

Fig. 2 Illustration of the conditions under which HDC mechanisms interfere with the accurate interpretation of TDA results for (A) 50 μm i.d. and (B) 25 μm i.d. capillaries. Red lines correspond to experimental conditions of constant analyte size (vertical) or constant mobilizing pressure (horizontal lines), and the dots represent experimental conditions investigated. Taylorgrams obtained from PS NPs with (C) constant analyte size at various mobilizing pressures and (D) constant mobilizing pressure with various analyte sizes. Note that deviations from Gaussian peak shape arise when experimental conditions enter the HDC regime, illustrated as shaded green region in (A) and (B). Adapted with permission from: J. Chamieh, L. Leclercq, M. Martin, S. Slaoui, H. Jensen, J. Østergaard, *et al.*, Limits in Size of Taylor Dispersion Analysis: Representation of the Different Hydrodynamic Regimes and Application to the Size-Characterization of Cubosomes, *Anal. Chem.*, 2017, **89**(24), 13487–13493. Copyright (2017) American Chemical Society.

integration method yielded a weight-average R_H determination. Furthermore, this method depended heavily on the selection of the boundaries for integration, defined by the variables n and m. Several boundaries were considered defined by cutoff lines ranging from 0–2% of the peak apex (Fig. 3A). Fig. 3B compares the results of the integration method (data points) with the results of conventional Gaussian fitting (horizontal dashed lines). A general trend of reduced mean R_H with increased cutoff percentage was observed. Comparison of the mean R_H values obtained from the integral and Gaussian fitting methods revealed no significant difference and agreement with 95% confidence. However, for third and fifth generation dendrigraft poly-L-lysine (G3 and G5), poor agreement was observed between the Gaussian fitting and integration methods at all cutoff percentages. The authors attributed this to Gaussian fitting being poorly suited for the irregular peak shapes of G3 and G5. To prevent contributions from noise influencing the integration method, the cutoff line corresponding to $4 \times \sigma_{noise}$ was defined as the appropriate threshold, which in this work corresponded to 0.75% of the peak apex (Fig. 3B, vertical dashed line).

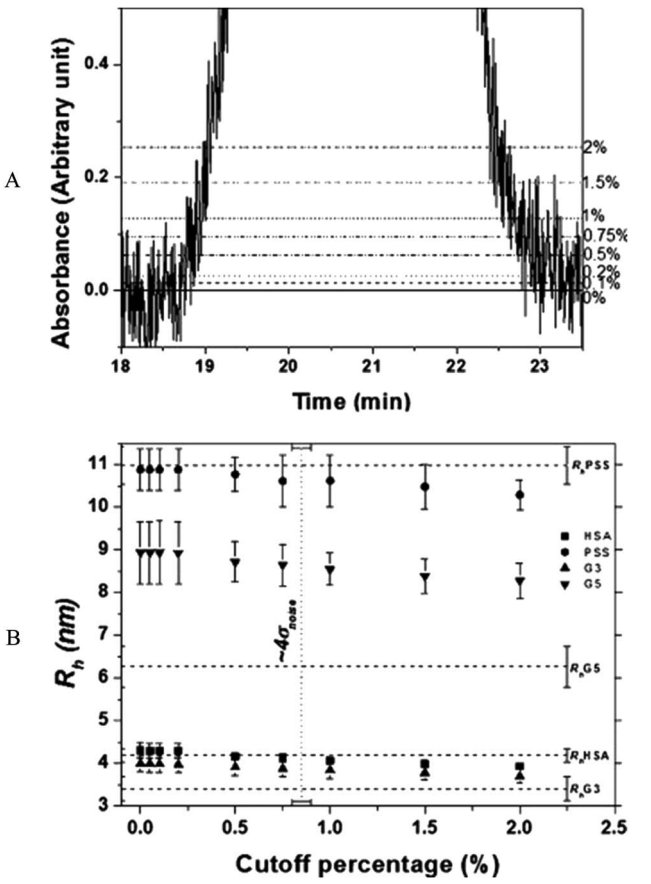

Fig. 3 Graphical representation of variance determination by peak integration. (A) Integration boundaries are represented by cut-off lines given as percentage of the peak apex (horizontal dashed lines); and (B) resulting trends in R_H measurements as a function of integration cut-off boundaries. The limiting cut-off boundary was determined to be 0.75% (vertical dashed line), which represented $4 \times \sigma_{noise}$. R_H measurements by the integration method (data points) are compared to standard Gaussian peak fitting values (horizontal dashed lines). Reprinted from Joseph Chamieh and Herve Cottet, Comparison of single and double detection points Taylor dispersion analysis for monodisperse and polydisperse samples, *J. Chromatogr. A*, 2012, **1241**, 123–127, Copyright (2012), with permission from Elsevier.

Data analysis methods have been developed to extract multiple constituent R_H values from the taylorgrams of mixtures.[15,55,56] In one example, three independent data analysis methods were applied to monitoring a polymerization reaction by TDA.[55] In the first method, the degree of conversion was determined by comparing integrated areas in the taylorgrams before and after the polymerization reaction. In the second method, the taylorgrams for each component in the reaction mixtures were recorded and fitted as Gaussian curves, and the taylorgram for the reaction mixture was deconvolved by fitting as the sum of Gaussian curves for the mixture components. The third method subtracted the Gaussian contribution of the monomer mixture from the taylorgram of the reaction mixture and fitted the reduced signal iteratively to extract the polymer contribution. Three standards of polyacrylamide (PAM) with varying weight average molar masses and acrylamide (AM) monomer were analyzed by TDA individually and as AM/PAM (10 : 90 v : v) mixtures for each molar mass standard to mimic a polymerization medium. Peak profiles in AM/PAM mixtures were shown to be the sum of the contributions from each component, as illustrated in Fig. 4A. All three data analysis methods determined $R_H = 0.22$ nm for AM, while R_H values for AM/PAM agreed across all methods to within 0.5 nm. TDA was performed on aliquots of an acrylamide polymerization reaction mixture at several time points, as illustrated in Fig. 4B. The three methods were separately utilized to determine R_H for the resulting PAM, and all methods agreed to within 4%.

Cipelletti described a cumulant analysis method for determining the polydispersity of moderately complex sample mixtures.[54] By the cumulant method, the logarithm of any taylorgram can be expanded into a cumulant series, in which the first cumulant (Γ_1) is directly related to the mean of the gamma distribution of D. The authors showed that polydispersity could be characterized by evaluating the deviation from linearity in the plot of the cumulant series. In further work, Cipelletti *et al.* described the constrained regularized linear inversion (CRLI) approach for determining probability density functions (PDFs) of D from taylorgrams.[44] This added additional constraints to the standard least-squares fit to overcome the difficulties of an infinite set of PDF solutions that fit the taylorgram function. D averages were determined by CRLI approach that agreed to within 10% of the expected values utilizing both simulated and experimental data, and up to 10% error was observed for determinations of polydispersity indices of various polystyrenesulfonate samples and mixtures.

Latunde-Dada *et al.* described an algorithmic approach to deconvolution of taylorgrams of mixtures based on initial parameter estimations as seed values for fitting by least squares regression.[57] In that approach, a system of equations describing the relative contributions of various peak amplitudes and variances can be solved using initial parameters derived from the second derivative, integral, and double integral of the net

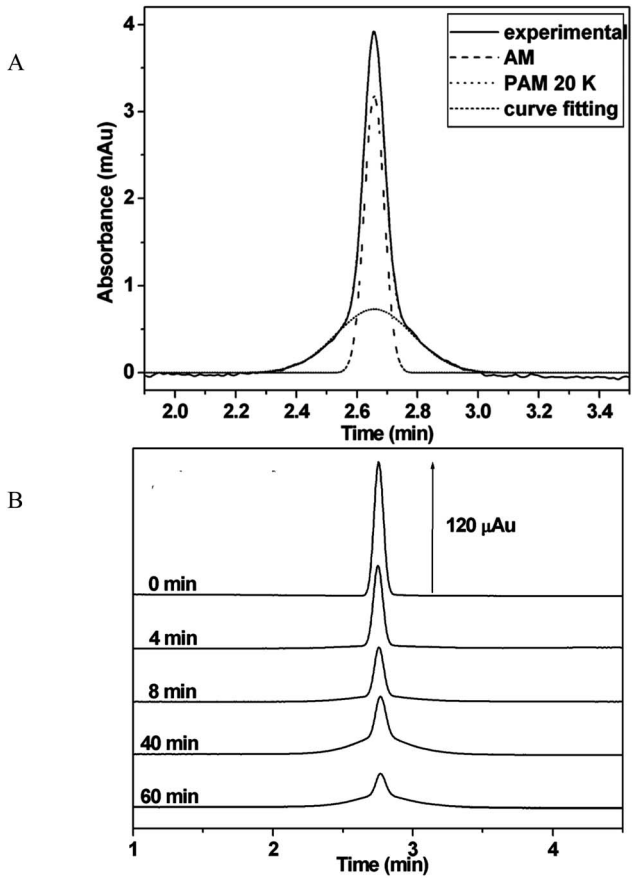

Fig. 4 (A) Taylorgram of an AM/PAM standard mixture with UV absorbance detection (solid line). The signal was deconvoluted by fitting to the sum of two Gaussian curves (dashed lines). (B) TDA time course profile of acrylamide polymerization with UV absorbance detection at 191 nm. Signal analysis using three methods based on conservation of mass of sample injection, deconvolution *via* Gaussian fits, and deconvolution *via* monomer contribution subtraction results in R_H determinations that agree to within 4%. Adapted with permission from: H. Cottet, J. P. Biron, L. Cipelletti, R. Matmour and M. Martin, Determination of Individual Diffusion Coefficients in Evolving Binary Mixtures by Taylor Dispersion Analysis: Application to the Monitoring of Polymer Reaction, *Anal. Chem.*, 2010, **82**(5), 1793–1802. Copyright (2010) American Chemical Society.

taylorgram signal. The authors demonstrated the utility of their approach in various use cases, including 2, 3, and 4 component mixtures of related and unrelated analytes, and with various conditions of *a priori* knowledge of analyte radius. In each case, hydrodynamic radii in good agreement with nominal reported values were determined for all mixture components.

These examples illustrate that fitting and deconvolution algorithms can be applied to interpreting taylorgrams of sample mixtures. Although no theoretical upper limit has been proposed for the number of mixture components that can be handled by these methods, the mathematical complexity and uncertainty inherent to such approaches suggests that they are best reserved for relatively simple mixtures. Applications requiring increased resolution and peak capacity will benefit from the common instrumentation shared by both CE and TDA, which facilitates their online integration.

Integrating CE and TDA

As we previously discussed, dual-point detection is an effective approach to circumventing challenges of non-uniform or discontinuous flow velocities in TDA, but it presents an engineering challenge of integrating two detection points within the confines of commercial CE instrumentation. Chamieh *et al.* implemented a dual-point UV detection approach by looping the capillary inside of a standard CE capillary cassette such that it passed the UV detection point twice before exiting the cassette (Fig. 5A).[17] This required modification of the instrument's detection interface to allow both detection windows on the looped capillary to overlap within the same interface. Fig. 5B (top) compares the taylorgrams obtained for 75 μM HSA using the unmodified interface (gray trace) and the modified interface (black trace). A 10-fold decrease in sensitivity was observed when using the modified detection interface, which the authors attributed to the removal of a spatial filtering slit which typically prevents transmission through the capillary in regions outside of the capillary inner diameter. However, reduced sensitivity did not adversely affect the observed peak variance or elution profiles of sufficiently concentrated samples, as observed by the normalized data in Fig. 5B (bottom). Dual-point UV detection was utilized to determine R_H at two mobilizing pressures (30 and 50 mbar, respectively) for 10 mM caffeine ($R_H = 0.462 \pm 0.013$ nm and 0.436 ± 0.017 nm), 75 μM BSA ($R_H = 4.10 \pm 0.12$ nm and 4.13 ± 0.13 nm), and 75 μM HSA ($R_H = 4.19 \pm 0.09$ nm and 4.25 ± 0.14 nm) and in all cases were found to agree with literature values to within 5%.

Fluorescence is often utilized as a detection mode in CE because it overcomes pathlength limitations of UV-absorbance detection in small diameter capillaries, but the integration of dual-point fluorescence detection in commercial CE instrumentation is challenging. Our group developed a miniature LED-induced fluorescence detection system for CE that was sufficiently compact to enable the integration of two detectors within the cassette of a commercial CE instrument.[16] The 3D printed design, shown in Fig. 5C incorporated an LED excitation source, bandpass excitation filter, pinhole collimator, and emission-collecting ball lens. Operating conditions such as LED current, and PMT gain control voltage were optimized *via* multivariate analysis to yield a detection limit of 613 ± 13 pM for fluorescein. The system was used to monitor the progress of a fluorescent bioconjugation reaction between fluorescein isothiocyanate (FITC) and BSA, and the integration of CE-TDA with fluorescence detection was shown to enable standard-free identification of peaks in the CE separation. Fig. 5D shows the overlay of signals obtained from both detectors (solid and dashed black traces) and the corresponding Gaussian fits (solid and dashed red traces) at reaction time = 2 min. TDA of the CE-separated zones provided R_H values of 4.4 nm and 0.54 nm for peak 1 and peak 2, respectively, allowing the assignment of these peaks to FITC–BSA and free FITC, respectively.

CE and TDA have been used together to monitor reaction progress in other systems. Affinity CE is widely utilized for studying biomolecular interactions, and in this regard CE-TDA

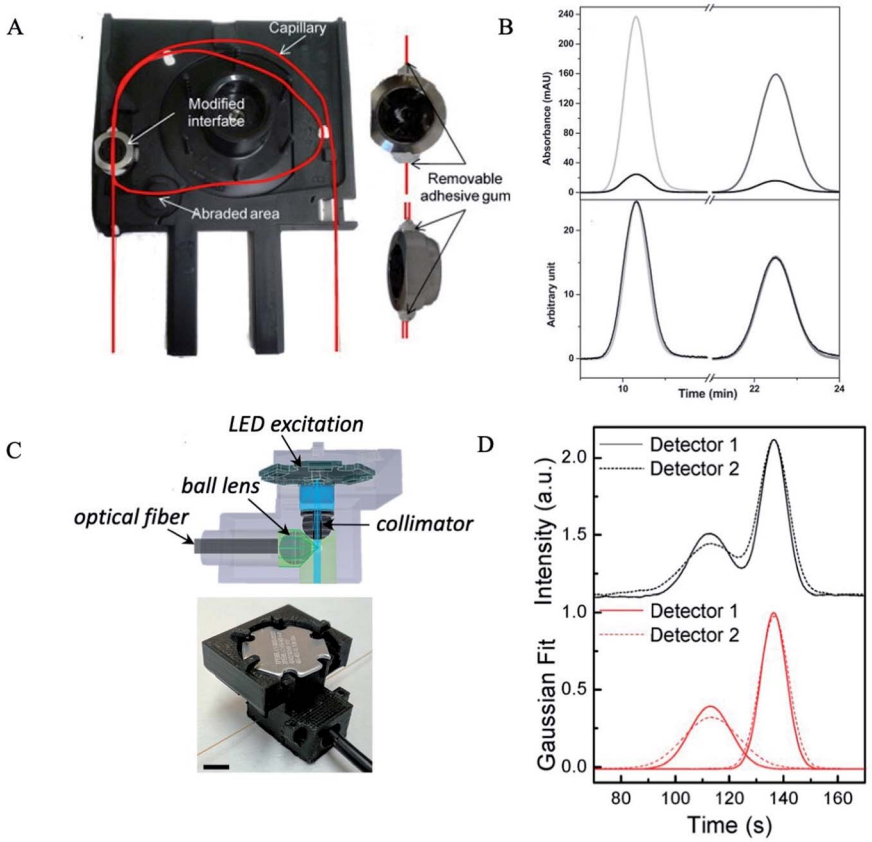

Fig. 5 (A) Illustration of a looped capillary within a standard CE instrument cassette for double detection TDA with UV absorbance detection. (B) Raw data (top) and normalized data (bottom) taylorgrams of HSA by conventional single-point UV absorbance detection interface (gray trace) and modified double detection interface (black trace). Note a dramatic reduction in sensitivity (*ca.* 10-fold) for the modified double detection interface. Normalized data shows no substantial difference in peak variance or elution time between detection methods. Adapted from Joseph Chamieh, Farid Oukacine and Herve Cottet, Taylor dispersion analysis with two detection points on a commercial capillary electrophoresis apparatus, *J. Chromatogr. A*, 2012, **1235**, 174–177, Copyright (2012), with permission from Elsevier. (C) Schematic illustration and photograph (scale bar is 5 mm) of a miniature 3D printed fluorescence detector for two-point fluorescence detection in a commercial CE instrument. (D) Raw (top) and Gaussian fitted (bottom) data from CE-TDA of FITC–BSA conjugation reaction. TDA determinations of R_H enabled peak assignments of FITC–BSA (first peak) and free FITC (second peak). Adapted with permission from: L. D. Casto, K. B. Do and C. A. Baker, A Miniature 3D Printed LED-Induced Fluorescence Detector for Capillary Electrophoresis and Dual-Detector Taylor Dispersion Analysis, *Anal. Chem.*, 2019, **91**(15), 9451–9457. Copyright (2019) American Chemical Society.

can offer advantages for elucidating biophysical and functional properties of binding systems. Østergaard and Jensen demonstrated the first application of CE-TDA for the simultaneous characterization of protein–ligand binding and protein R_H in two separate affinity systems.[76] Advancing fronts were used to obtain D and R_H values for free ligands, α_1-acid glycoprotein (AGP) and human serum albumin (HSA), and for propranolol–ligand complexes to investigate and quantify their interactions. Differences in the degree of binding between propranolol–AGP and propranolol–HSA were significantly different, showing a trend in agreement with previous literature. Further, Liu *et al.* monitored surface functionalization of dendrigraft poly-L-lysines (DGL).[91] TDA was used to determine the R_H of the polypeptides and of a click reaction product. While the results confirmed the reaction, TDA gives a weight average R_H which does not provide information on reagent or product purity nor homogeneity. CE was used separately from, and complimentary to, TDA to characterize the reaction mixture components. Comparison of electropherograms of the clicked product spiked with the starting materials and intermediate compounds clearly illustrated the absence of these reaction components in the final product. Similarly, Deschamps *et al.* characterized the size of an ionic polydiacetylene by TDA while monitoring its polymerization process by CE.[92] R_H values for the polymer were reported as 1.77 nm and 1.9 nm by TDA and DLS, respectively, where the small difference was attributed to sample polydispersity. CE results were used in this study to determine degree of polymerization, polydispersity index, and number average molar mass. CE is also well-suited for online integration with TDA, which combines in a single analysis the high resolving power of CE with R_H determinations by TDA.[93] A mixture can be electrophoretically separated with high resolution while experimental traces from the same detector are recorded and used for TDA. Several groups have reported success in on-line integration of CE-TDA for monitoring of bioconjugation reactions,[16,76] nanoparticle characterization,[49,50,78,94] characterization of charged complexes,[93,95] and more.

Characterizing the 3D structure of proteins and biomolecules is critical in understanding their biological function. Xu and coworkers developed mobility capillary electrophoresis (MCE) to circumvent challenges associated with common structural analysis techniques.[96,97] MCE combines CE with suppressed electroosmotic flow and TDA to enable determinations of R_H and effective ionic charge from a single experiment. MCE has been demonstrated in combination with mass spectrometry and molecular dynamics simulations for 3D protein structural analysis from solution-phase samples. MCE has been applied to a variety of proteins and protein mixtures, under native conditions and non-native pH conditions.[98,99]

The characterization of size and function in non-biological systems by CE-TDA has also been reported. Leclercq and Cottet proposed a methodology for the characterization of polyelectrolyte complexes in which a CE separation of constituents followed by TDA allows for the determination of charge stoichiometry and R_H, respectively.[95] Oukacine *et al.* utilized the high separation performance of CE in conjunction with the absolute size determination of TDA for the determination of R_H of a bimodal mixture of nanolatexes (56 and 70 nm in size).[78] First, a baseline separation of the two nanolatexes by CE was required before TDA could be performed. A UV detector and capillary with three detection windows in a looped configuration was used in this study. Reported values of D were in good agreement with values obtained by TDA of the two nanolatexes individually, ultimately demonstrating CE-TDA as a suitable approach for the characterization of mixtures of nanoparticles similar in size.

Applications of TDA to bioanalysis

Analysis of biological and pharmaceutical compounds can take advantage of the low sample volumes of TDA, since sample availability in these cases can be limiting.[54] Such compounds include therapeutic peptides and proteins,[26–29,31–35] drug delivery systems,[30,37,38] and lipids.[39–42] Diffusion and transport through tissue mimics, hydrogels, and capillaries has also been modeled for biological applications.[30,31,100]

Hulse *et al.* demonstrated TDA for the size characterization of therapeutic proteins and their respective aggregates.[28] 60 nL of 10 mg mL^{-1} bovine serum albumin (BSA) were prepared and analyzed in less than 3 minutes using a commercial TDA instrument. R_H was determined to be 4.18 nm with an RSD of 0.24%, which was in agreement with previously reported values of 3.3–4.3 nm. Aggregation was induced in two samples of BSA *via* heat stress. Comparing average R_H values of BSA determined by DLS and TDA, it was determined that greater repeatability was achieved with TDA, indicated by <1% RSD as compared to 7.09% RSD by DLS in each aggregated sample.

Høgstedt *et al.* assessed protein–protein and peptide–peptide interactions (PPIs) by TDA.[27] PPIs can be characterized by the diffusion interaction parameter, k_D, which is observed as the slope of the linear fit in a plot of D *vs.* analyte concentration. A comparison of TDA and DLS for characterizing PPIs in model peptides was not possible since, the authors reported, DLS lacked appropriate detection sensitivity for the model peptides. Therefore, TDA and DLS were compared for characterizing PPIs for the proteins α-lactalbumin and HSA with highly comparable results. The higher sensitivity of TDA enabled observation of repulsive and attractive PPIs in a set of three model peptides. Furthermore, Latunde-Dada *et al.* proposed a method for obtaining concentration dependent diffusion coefficients and k_D in a single measurement by measuring dispersion as a function of concentration along the front of a sample slug.[18] For the application to caffeine and BSA solutions, the values and signs of k_D as well as the values of D were in good agreement with literature values and DLS results.

Protein–ligand interactions have also been studied by TDA coupled to mass spectrometry (TDA-MS). Hong *et al.* investigated noncovalent interactions of lysozyme and cytochrome C with tri-*N*-acetylchitotriose.[87] A home-built sample introduction system utilizing branched capillary channels and constant pressure pumping enabled two-point detection TDA-MS *via* electrospray ionization. Peaks corresponding to the protein, ligand, and the protein–ligand complex were well resolved by MS, and effective charges were determined. Ion chromatograms from the mass spectra were used for R_H determinations by TDA. TDA results showed a 6.963% and 7.53% increase in R_H of lysozyme and cytochrome C, respectively, after incubation with the ligand, indicative of protein–ligand binding.

Nanoscale hydrogels are utilized as drug delivery systems, enabling spatial, temporal, and stimulus-controlled drug release. Size characterization of these nanogel delivery systems is important, since size distribution influences *in vivo* diffusion, biodistribution, and ultimately the biological fate of these drug delivery vehicles.[30] Several studies have been successful in characterizing these drug delivery systems *via* TDA. Ibrahim *et al.* have worked to characterize the size and effective charge of a polymeric nanogel by TDA and CE, respectively.[30] Four copolymer nanogels were sized by TDA, resulting in an RSD of <2.2% for all R_H values, while effective ionic charge (z_{eff}) was determined for each nanogel from electrophoretic mobility and R_H. Jensen *et al.* have also studied hydrogel matrices as drug delivery systems, but as a subcutaneous tissue mimic.[31] A UV imaging method was combined with TDA to visualize and characterize diffusivity and self-association behavior of insulin within an agarose hydrogel matrix in real-time. At various concentrations, insulin monomers and hexamers were easily distinguished by TDA. Low concentrations (0.1 and 0.2 mM) and pH (3.0) resulted in $R_H = 1.5 \pm 0.1$ nm, representing the monomeric form of insulin, and high concentrations (1 mM) and moderate pH (7.4) resulted in $R_H = 3.0 \pm 0.1$ nm, indicative of the insulin hexamer. The authors reported that DLS was less sensitive to these small changes in hydrodynamic radius.

Ye *et al.* demonstrated the application of TDA to characterizing D and R_H values of drug substances in water and various pharmaceutical media (acetonitrile, methanol, isopropyl myristate, medium chain triglyceride, and propylene glycol), along with simultaneous measurements of solvent viscosity.[37] Relative solvent viscosity measurements were made using the two detection windows and water as a reference viscosity standard by the following equation:

$$\eta = \frac{\eta_{water}(t_{2,s} - t_{1,s})}{t_{2,water} - t_{1,water}} \quad (17)$$

where η is the relative solvent viscosity, η_{water} is water viscosity, $t_{1,s}$ and $t_{2,s}$ are the times at which the analyte in the solvent reaches detection windows 1 and 2, respectively, and $t_{1,water}$ and $t_{2,water}$ are the times at which the analyte in water reaches detection windows 1 and 2, respectively. Viscosity was determined for all solvents with RSD <1%. This work highlights the importance of considering solvent viscosity in R_H determinations, since D significantly decreases with increasing solvent viscosity, which can lead to overestimation of R_H. Simultaneous determination of solvent viscosity and D by TDA offers a promising approach to circumventing this problem.

Surfactant micelles or microemulsions are used as drug delivery systems to improve the solubility and bioavailability of drugs with poor water solubility. Formulations of these lipid-based excipients can be complex and, as with other drug delivery systems, their size characteristics will impact the efficacy of the drug delivery system. Chamieh *et al.* have made significant contributions to the characterization of micelles and microemulsions by TDA. TDA is well suited to this purpose because it is less sensitive than DLS to deleterious effects from aggregates, and variation in viscosity of micellar solutions can readily be accounted for. The effect of concentration and temperature on the size of commercial self-emulsifying pharmaceutical excipients was investigated by TDA and results compared to DLS measurements. The two excipients studied, Labrasol®[40] and Gelucire® 44/14,[39] were found to have opposite trends in behavior based on concentration and temperature; Labrasol® microemulsions showed a decrease in the measured R_H (90 nm to 6 nm) with increased concentration, while Gelucire® 44/14 showed an increase in measured R_H (1 nm to 5.5 nm) with increased concentration. The authors postulate that this opposite trend was due to coacervation in low concentrations of Labrasol® and increase in viscosity of higher concentrations of Gelucire® 44/14.

An often-important criteria for drug delivery systems is the ability to keep the loaded drug inside the prepared emulsion or droplet solution in the gastrointestinal tract, where digestive enzymes are present. In continuation of their previous studies, Chamieh *et al.* monitored the size of excipients during *in vitro* lipolysis under conditions simulating the gastrointestinal tract.[41] Digestion of the excipients were monitored by TDA at several time points in the degradation process. Similar to their previous work, an opposite behavior was observed, as Labrasol® droplets decrease in size (Fig. 6A and B), due to the disappearance of coacervates that are unable to solubilize the hydrophobic fluorescent marker and Gelucire® droplets increase in size during lipolysis (Fig. 6C and D) due to the increase in micelle size, maintaining solubilizing capacity. TDA was shown to be effective for size analysis of microemulsions and their behavior under digestive conditions. TDA is also an effective method for quantifying peptide drugs released from lipidic self-emulsifying drug delivery systems. The role of electrolyte ionic strength on the release of two therapeutic peptides, leuprorelin and desmopressin has also been characterized.[26]

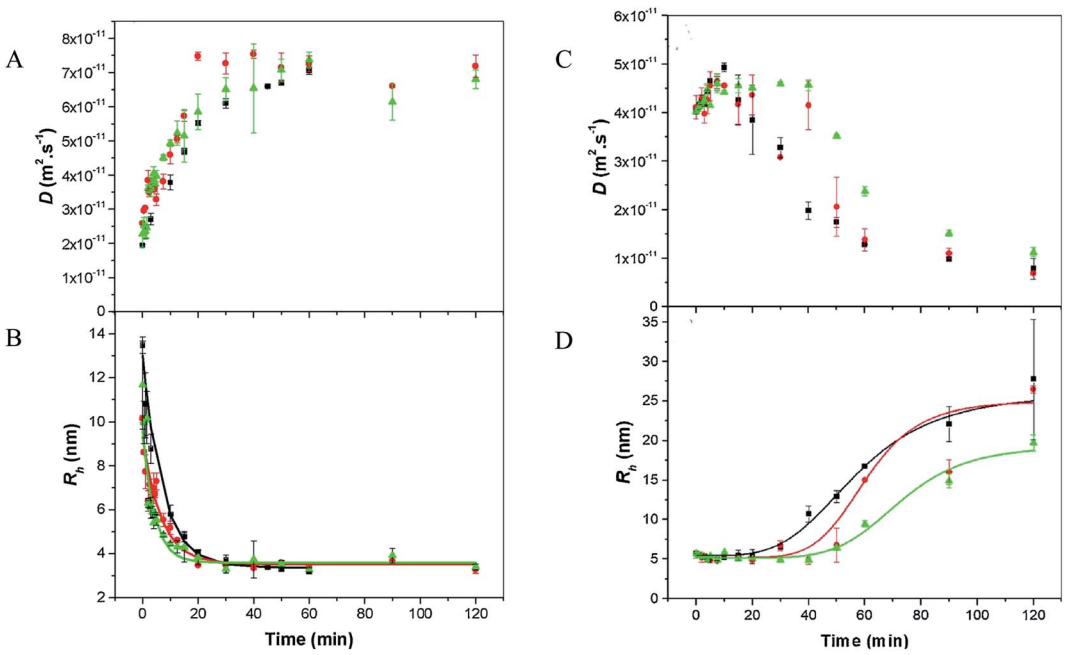

Fig. 6 Graphical comparison of diffusion coefficients and hydrodynamic radii of Labrasol® and Gelucire® droplets during lipolysis at 37 °C. (A) D measurements of Labrasol® droplets are shown to increase and (B) corresponding R_H values decrease exponentially before reaching a plateau. (C) D measurements of Gelucire® droplets are shown to decrease and (D) corresponding R_H values increase sigmoidally. Adapted from Joseph Chamieh, Habib Merdassi, Jean-Christophe Rossi, Vincent Jannin, Frederic Demarne and Herve Cottet, Size characterization of lipid-based self-emulsifying pharmaceutical excipients during lipolysis using Taylor dispersion analysis with fluorescence detection, *Int. J. Pharm.*, 2018, **537**, 94–101, Copyright (2018), with permission from Elsevier.

TDA applications in nanomaterials characterization

Physiochemical properties of inorganic nanoparticles (NPs) are primarily dependent on their size, and TDA has proven well-suited for characterizing NPs. Sizing of NPs by TDA has been well-studied and has demonstrated utility.[43–51] NP size characterization by TDA has been compared to TEM imaging techniques and found to result in comparable particle size values. For example, Balog *et al.* studied superparamagnetic iron oxide NPs (SPIONs), gold (Au) NPs, and silica (SiO_2) NPs and compared TDA to TEM in determination of particle radius.[43] The reported radii of SPIONs, Au NPs, and SiO_2 NPs were 7.6 nm, 33.8 nm, and 44.0 nm, respectively, by TDA, and 6.7 ± 1.1 nm, 28.0 ± 4.7 nm, and 39.3 ± 6.2 nm, respectively, by TEM.

Sizing is also useful in characterizing the modification of NPs with adsorbed functional components such as enzymes. Holdrich *et al.* investigated pepsin coated gold nanoparticles by DLS and TDA.[47] Pepsin was adsorbed onto synthesized gold nanoparticles (GNPs), with a DLS measured diameter of 44.1 ± 0.3 nm, at varying concentrations to obtain a range of thicknesses of the adsorbed layer. The average hydrodynamic diameter of pepsin-coated GNPs by DLS was reported as 64 ± 2 nm, where the GNPs synthesized with different concentrations of the pepsin coating solution were not significantly different. This suggests that DLS was unable to successfully distinguish the small differences in hydrodynamic diameter of the pepsin–GNP bioconjugates as compared to bare GNPs (Fig. 7A), while TDA successfully resolved increases in R_H due to pepsin adsorption as small as <2 nm with a high degree of repeatability and accuracy (Fig. 7B).

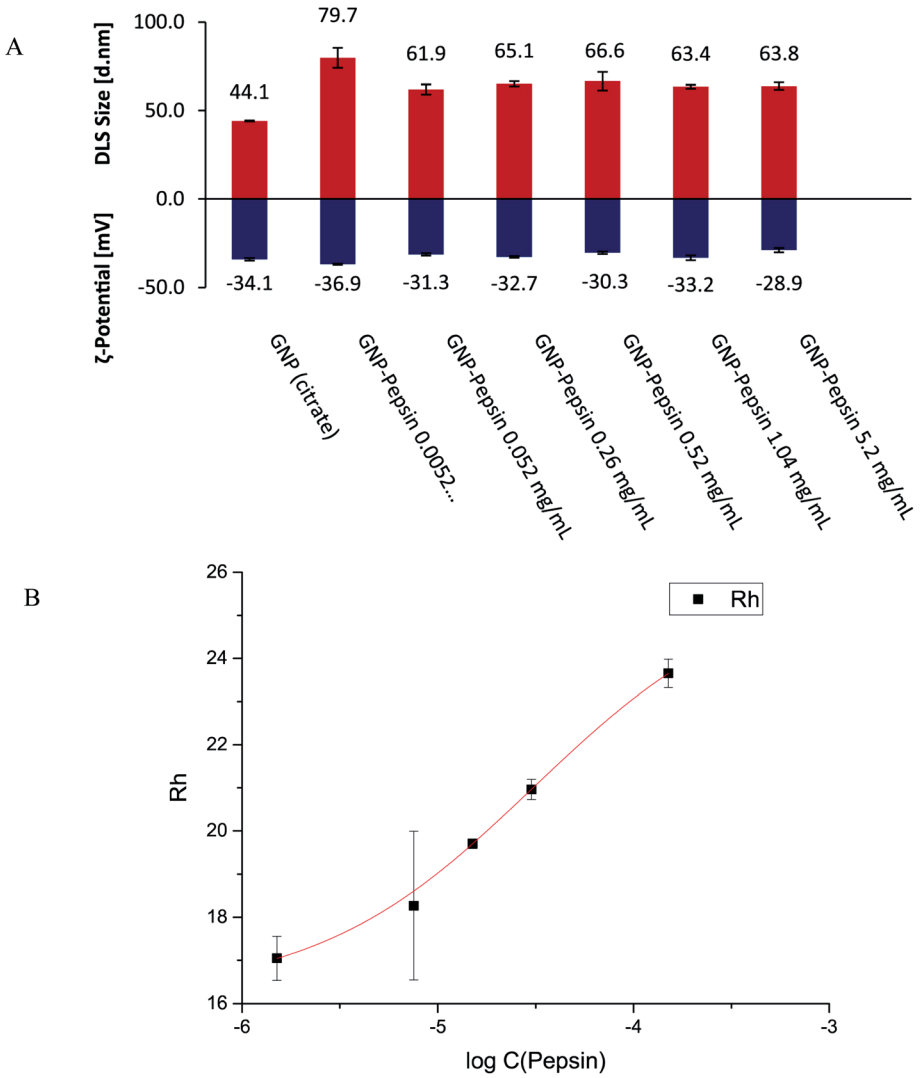

Fig. 7 Comparison of (A) DLS measurements for hydrodynamic diameters and (B) TDA measurements for R_H of pepsin-coated GNPs at varying concentrations of pepsin. While increasing diameter of pepsin-functionalized GNPs was expected with increasing pepsin concentration, DLS did not resolve the small size differences of bioconjugates prepared at various pepsin concentrations. TDA resolved the trend of increasing R_H with increasing pepsin concentration. Adapted from Markus Holdrich, Siyao Liu, Markus Epe and Michael Lammerhofer, Taylor dispersion analysis, resonant mass measurement and bioactivity of pepsin-coated gold nanoparticles, *Talanta*, 2017, **167**, 67–74, Copyright (2017), with permission from Elsevier.

Size characterization is also important for understanding organic materials, for observing polymer synthesis and degradation, ligand binding, and monitoring reaction progress. The utility of UV and fluorescence detection modes for TDA are discussed previously in this review. In many situations pertinent to organic synthesis, however, molecules may exhibit neither significant UV absorption nor fluorescence. Refractive index (RI) detection is a potential alternative in these cases, and RI detection has been used for TDA performed with HPLC instrumentation, but these examples required detection volumes on the order of 10 μL, which eliminates the key advantages of small sample volumes and reduced analysis times in TDA.[62,101,102] Saetear *et al.* developed a backscattering interferometry (BSI) approach to improve RI detection in TDA with nanoliter sample volumes.[89] A selection of poly- and monosaccharides, which present a significant detection challenge due to low UV absorbance, were characterized by TDA using the BSI technique in a commercial CE instrument. Determinations of D gave an average RSD of 2%, demonstrating high repeatability in the TDA-BSI analyses of non-UV absorbing molecules. In continuation of this study, Leclercq *et al.* investigated a UV-photooxidation (UV-POD) detection mode for TDA of polysaccharides and compared results to the BSI method, as detection sensitivity of TDA-BSI is relatively low (LOD ≈ 50–80 mg L^{-1}).[22] R_H values for a selection of polysaccharides were determined by TDA-BSI and TDA-UV-POD with an average relative difference in R_H between the two detection modes of ~2% and an RSD below 3%. Additionally, detection sensitivity of TDA-UV-POD for pullulans and dextrans was greater than that of TDA-BSI (LOD = 40 mg L^{-1} and 50–60 mg L^{-1}, respectively). These works expand the applications of TDA to applications requiring universal detection modes.

Characterizing the degradation products of biopolymers is essential for understanding the fate of these materials in biomedical applications. The application of TDA to monitoring hydrolytic degradation of a fifth generation dendrigraft poly-L-lysine (DGL G5) has been described.[60] Using three different approaches – curve fitting, cumulant series expansion, and constrained regularized linear inversion – R_H values were obtained at different degradation times. The R_H value for the enzymatic degradation of DGL n corresponds to the R_H of the n-1 generation, elucidating structural and behavioral information about the polymer and enzyme, such as reaction kinetics and degradation process. Other biopolymers, such as natural rubber,[103] polyplexes,[21] and the influence of ionic strength[104] on these systems have also been studied by TDA.

Conclusion

In this review, we aimed to illustrate TDA as a powerful sizing technique that offers comparable sizing performance with reduced sample consumption and often improved detection sensitivity as compared to more common sizing techniques such as DLS, SEC, or various imaging approaches. First, we offered a tutorial on the fundamental principles that allow TDA to achieve calibration-free sizing of analytes across a wide range of R_H, with an emphasis on the reduced sample consumption and analysis times that result from utilizing fused silica capillaries. We continued by highlighting relationships between operating parameters, such as u and R_c, and the critically important Taylor conditions. Our intention was to acquaint those seeking to utilize TDA with the careful consideration needed to design effective TDA experiments. Our discussion continued by looking at methods for applying TDA to sample mixtures, first *via* algorithmic approaches, then by looking at the integration of CE and TDA. Finally, we presented a selection of reports that demonstrate TDA applied to complex challenges in bioanalysis and materials science.

TDA is a particularly attractive analytical method because it achieves calibration-free sizing across an impressive dynamic range (*ca.* Å to μm) while utilizing nL sample volumes and straightforward and accessible instrumentation. We see a valuable opportunity to expand the adoption of this technology within the broader separation science community. Meeting that opportunity requires effort in a few areas. First, wider dissemination of the principles and capabilities of TDA are needed, towards which we offer the current tutorial review. Second, navigating the relationship between operating parameters and meeting the Taylor conditions is a barrier to entry for those with little or no prior experience in TDA. This barrier would be substantially lowered by making available adaptable, open-source calculation tools. Third, although TDA can be readily achieved with commercial CE instrumentation, the cost of these instruments is not trivial, and their capabilities far exceed the minimum requirements for typical TDA analysis. Therefore, those without a CE instrument may not be inclined to acquire one for the sole purpose of TDA, and those with a CE instrument may find its broader capabilities put to more efficient use for other purposes. A few TDA-specific instruments are commercially available, but the cost may be yet another barrier to entry. Ultimately, TDA is a mechanistically simple measurement to implement, which may be amenable to the development of low-cost, open-source hardware that will enable wide adoption of this powerful analytical method. We believe that wider adoption of TDA will enable new dimensions of analysis across various sub-fields of analytical chemistry and measurement science.

Conflicts of interest

There are no conflicts of interest to declare.

Acknowledgements

The authors were supported by funds from the National Institute of General Medical Sciences of the National Institutes of Health under award number R35GM138173, and by by the National Science Foundation under grant number CHE-2054748.

References

1 A. S. Lawrie, A. Albanyan, R. A. Cardigan, I. J. Mackie and P. Harrison, Microparticle sizing by dynamic light

scattering in fresh-frozen plasma, *Vox Sang.*, 2009, **96**(3), 206–212.
2 L. L. Chaikov, M. N. Kirichenko, S. V. Krivokhizha and A. R. Zaritskiy, Dynamics of statistically confident particle sizes and concentrations in blood plasma obtained by the dynamic light scattering method, *J. Biomed. Opt.*, 2015, **20**(5), 7.
3 J. Stetefeld, S. A. McKenna and T. R. Patel, Dynamic light scattering: a practical guide and applications in biomedical sciences, *Biophys. Rev.*, 2016, **8**(4), 409–427.
4 A. Hawe, W. L. Hulse, W. Jiskoot and R. T. Forbes, Taylor Dispersion Analysis Compared to Dynamic Light Scattering for the Size Analysis of Therapeutic Peptides and Proteins and Their Aggregates, *Pharm. Res.*, 2011, **28**(9), 2302–2310.
5 T. Arakawa, D. Ejima, T. S. Li and J. S. Phil, The Critical Role of Mobile Phase Composition in Size Exclusion Chromatography of Protein Pharmaceuticals, *J. Pharm. Sci.*, 2010, **99**(4), 1674–1692.
6 V. Pacáková, K. Stulik, P. T. Hau, I. Jelinek, I. Vins and D. Sykora, Comparison of High-Performance Liquid-Chromatography and Capillary Electrophoresis for the Determination of Some Bee Venom Components, *J. Chromatogr. A*, 1995, **700**(1–2), 187–193.
7 R. D. Ricker and L. A. Sandoval, Fast, reproducible size-exclusion chromatography of biological macromolecules, *J. Chromatogr. A*, 1996, **743**(1), 43–50.
8 A. Bootz, V. Vogel, D. Schubert and J. Kreuter, Comparison of scanning electron microscopy, dynamic light scattering and analytical ultracentrifugation for the sizing of poly(butyl cyanoacrylate) nanoparticles, *Eur. J. Pharm. Biopharm.*, 2004, **57**(2), 369–375.
9 C. Hegel, C. Jones, F. Cabrera, M. J. Yanez and V. Bucala, Particle Size Characterization: Comparison of Laser Difraction (LD) and Scanning Electron Microscopy (SEM), *Acta Microsc.*, 2014, **23**(1), 11–17.
10 V. Sokolova, A. K. Ludwig, S. Hornung, O. Rotan, P. A. Horn, M. Epple, *et al.*, Characterisation of exosomes derived from human cells by nanoparticle tracking analysis and scanning electron microscopy, *Colloids Surf., B*, 2011, **87**(1), 146–150.
11 W. Haiss, N. T. K. Thanh, J. Aveyard and D. G. Fernig, Determination of size and concentration of gold nanoparticles from UV-Vis spectra, *Anal. Chem.*, 2007, **79**(11), 4215–4221.
12 Z. L. Wang, Transmission electron microscopy of shape-controlled nanocrystals and their assemblies, *J. Phys. Chem. B*, 2000, **104**(6), 1153–1175.
13 R. Garcia and R. Perez, Dynamic atomic force microscopy methods, *Surf. Sci. Rep.*, 2002, **47**(6–8), 197–301.
14 J. Grobelny, F. W. DelRio, N. Pradeep, D. I. Kim, V. A. Hackley and R. F. Cook, Size Measurement of Nanoparticles Using Atomic Force Microscopy, in *Characterization of Nanoparticles Intended for Drug Delivery, Methods in Molecular Biology*, ed. S. E. McNeil, Humana Press Inc, Totowa, 2011, vol. 697, pp. 71–82.
15 H. Cottet, J. P. Biron and M. Martin, Taylor dispersion analysis of mixtures, *Anal. Chem.*, 2007, **79**(23), 9066–9073.
16 L. D. Casto, K. B. Do and C. A. Baker, A Miniature 3D Printed LED-Induced Fluorescence Detector for Capillary Electrophoresis and Dual-Detector Taylor Dispersion Analysis, *Anal. Chem.*, 2019, **91**(15), 9451–9457.
17 J. Chamieh, F. Oukacine and H. Cottet, Taylor dispersion analysis with two detection points on a commercial capillary electrophoresis apparatus, *J. Chromatogr. A*, 2012, **1235**, 174–177.
18 S. Latunde-Dada, R. Bott, D. Barker and O. I. Leszczyszyn, Methodologies for the rapid determination of the diffusion interaction parameter using Taylor dispersion analysis, *Anal. Methods*, 2016, **8**(2), 386–392.
19 C. Secuianu, G. C. Maitland, J. P. M. Trusler and W. A. Wakeham, Mutual Diffusion Coefficients of Aqueous KCl at High Pressures Measured by the Taylor Dispersion Method, *J. Chem. Eng. Data*, 2011, **56**(12), 4840–4848.
20 G. S. Zhuang, N. N. Poulsen, N. J. Petersen, J. Østergaard and H. Jensen, *A Capillary-based Microfluidic Device Incorporating Optical Fibers for Flow Induced Dispersion Analysis*, IEEE, 2013, pp. 1054–1057.
21 L. Leclercq, S. Reinhard, J. Chamieh, M. Doblinger, E. Wagner and H. Cottet, Fast Characterization of Polyplexes by Taylor Dispersion Analysis, *Macromolecules*, 2015, **48**(19), 7216–7221.
22 L. Leclercq, P. Saetear, A. Rolland-Sabate, J. P. Biron, J. Chamieh, L. Cipelletti, *et al.*, Size-Based Characterization of Polysaccharides by Taylor Dispersion Analysis with Photochemical Oxidation or Backscattering Interferometry Detections, *Macromolecules*, 2019, **52**(12), 4421–4431.
23 G. Taylor, Dispersion of Soluble Matter in Solvent Flowing Slowly Through a Tube, *Proc. R. Soc. London*, 1953, **219**(1137), 186–203.
24 G. Taylor, The Dispersion of Matter in Turbulent Flow Through a Pipe, *Proc. R. Soc. London, Ser. A*, 1954, **223**(1155), 446–468.
25 J. C. Giddings and S. L. Seager, Rapid Determination of Gaseous Diffusion Coefficients by means of Gas Chromatography Apparatus, *J. Chem. Phys.*, 1960, **33**(5), 1579–1580.
26 J. Chamieh, A. D. Tarrat, C. Doudou, V. Jannin, F. Demarne and H. Cottet, Peptide release from SEDDS containing hydrophobic ion pair therapeutic peptides measured by Taylor dispersion analysis, *Int. J. Pharm.*, 2019, **559**, 228–234.
27 U. B. Høgstedt, G. Schwach, M. van de Weert and J. Østergaard, Taylor dispersion analysis as a promising tool for assessment of peptide-peptide interactions, *Eur. J. Pharm. Sci.*, 2016, **93**, 21–28.
28 W. Hulse and R. Forbes, A Taylor dispersion analysis method for the sizing of therapeutic proteins and their aggregates using nanolitre sample quantities, *Int. J. Pharm.*, 2011, **416**(1), 394–397.

29 W. L. Hulse, J. Gray and R. T. Forbes, Evaluating the inter and intra batch variability of protein aggregation behaviour using Taylor dispersion analysis and dynamic light scattering, *Int. J. Pharm.*, 2013, **453**(2), 351–357.
30 A. Ibrahim, R. Meyrueix, G. Pouliquen, Y. P. Chan and H. Cottet, Size and charge characterization of polymeric drug delivery systems by Taylor dispersion analysis and capillary electrophoresis, *Anal. Bioanal. Chem.*, 2013, **405**(16), 5369–5379.
31 S. S. Jensen, H. Jensen, C. Cornett, E. H. Moller and J. Østergaard, Insulin diffusion and self-association characterized by real-time UV imaging and Taylor dispersion analysis, *J. Pharm. Biomed. Anal.*, 2014, **92**, 203–210.
32 A. Lavoisier and J. M. Schlaeppi, Early developability screen of therapeutic antibody candidates using Taylor dispersion analysis and UV area imaging detection, *mAbs*, 2015, **7**(1), 77–83.
33 N. N. Poulsen, N. Z. Andersen, J. Østergaard, G. S. Zhuang, N. J. Petersen and H. Jensen, Flow induced dispersion analysis rapidly quantifies proteins in human plasma samples, *Analyst*, 2015, **140**(13), 4365–4369.
34 N. N. Poulsen, M. E. Pedersen, J. Østergaard, N. J. Petersen, C. T. Nielsen, N. H. H. Heegaard, *et al.*, Flow-Induced Dispersion Analysis for Probing Anti-dsDNA Antibody Binding Heterogeneity in Systemic Lupus Erythematosus Patients: Toward a New Approach for Diagnosis and Patient Stratification, *Anal. Chem.*, 2016, **88**(18), 9056–9061.
35 M. Zuo and Y. Chen, Fast determination of protein diffusion coefficient by Taylor dispersion analysis and capillary electrophoresis system, *Chem. J. Chin. Univ.*, 2007, **28**(10), 1875–1877.
36 M. S. Restan, M. E. Pedersen, H. Jensen and S. Pedersen-Bjergaard, Electromembrane Extraction of Unconjugated Fluorescein Isothiocyanate from Solutions of Labeled Proteins Prior to Flow Induced Dispersion Analysis, *Anal. Chem.*, 2019, **91**(10), 6702–6708.
37 F. B. Ye, H. Jensen, S. W. Larsen, A. Yaghmur, C. Larsen and J. Østergaard, Measurement of drug diffusivities in pharmaceutical solvents using Taylor dispersion analysis, *J. Pharm. Biomed. Anal.*, 2012, **61**, 176–183.
38 H. Zaman, A. G. Bright, K. Adams, D. M. Goodall and R. T. Forbes, Characterisation of aggregates of cyclodextrin-drug complexes using Taylor dispersion analysis, *Int. J. Pharm.*, 2017, **522**(1–2), 98–109.
39 J. Chamieh, F. Davanier, V. Jannin, F. Demarne and H. Cottet, Size characterization of commercial micelles and microemulsions by Taylor dispersion analysis, *Int. J. Pharm.*, 2015, **492**(1–2), 46–54.
40 J. Chamieh, V. Jannin, F. Demarne and H. Cottet, Hydrodynamic size characterization of a self-emulsifying lipid pharmaceutical excipient by Taylor dispersion analysis with fluorescent detection, *Int. J. Pharm.*, 2016, **513**(1–2), 262–269.
41 J. Chamieh, H. Merdassi, J. C. Rossi, V. Jannin, F. Demarne and H. Cottet, Size characterization of lipid-based self-emulsifying pharmaceutical excipients during lipolysis using Taylor dispersion analysis with fluorescence detection, *Int. J. Pharm.*, 2018, **537**(1–2), 94–101.
42 J. Petr, Rapid determination of the critical micelle concentration by Taylor dispersion analysis in capillaries using both direct and indirect detection, *J. Sep. Sci.*, 2017, **40**(6), 1421–1426.
43 S. Balog, D. A. Urban, A. M. Milosevic, F. Crippa, B. Rothen-Rutishauser and A. Petri-Fink, Taylor dispersion of nanoparticles, *J. Nanopart. Res.*, 2017, **19**(8), 287.
44 L. Cipelletti, J. P. Biron, M. Martin and H. Cottet, Measuring Arbitrary Diffusion Coefficient Distributions of Nano-Objects by Taylor Dispersion Analysis, *Anal. Chem.*, 2015, **87**(16), 8489–8496.
45 F. d'Orlye, A. Varenne and P. Gareil, Determination of nanoparticle diffusion coefficients by Taylor dispersion analysis using a capillary electrophoresis instrument, *J. Chromatogr. A*, 2008, **1204**(2), 226–232.
46 P. Hajiani and F. Larachi, Reducing Taylor dispersion in capillary laminar flows using magnetically excited nanoparticles: nanomixing mechanism for micro/nanoscale applications, *Chem. Eng. J.*, 2012, **203**, 492–498.
47 M. Holdrich, S. Y. Liu, M. Epe and M. Lammerhofer, Taylor dispersion analysis, resonant mass measurement and bioactivity of pepsin-coated gold nanoparticles, *Talanta*, 2017, **167**, 67–74.
48 P. Lemal, A. Petri-Fink and S. Balog, Nanoparticles and Taylor Dispersion as a Linear Time-Invariant System, *Anal. Chem.*, 2019, **91**(2), 1217–1221.
49 U. Pyell, A. H. Jalil, C. Pfeiffer, B. Pelaz and W. J. Parak, Characterization of gold nanoparticles with different hydrophilic coatings via capillary electrophoresis and Taylor dispersion analysis. Part I: determination of the zeta potential employing a modified analytic approximation, *J. Colloid Interface Sci.*, 2015, **450**, 288–300.
50 U. Pyell, A. H. Jalil, D. A. Urban, C. Pfeiffer, B. Pelaz and W. J. Parak, Characterization of hydrophilic coated gold nanoparticles via capillary electrophoresis and Taylor dispersion analysis. Part II: determination of the hydrodynamic radius distribution - comparison with asymmetric flow field-flow fractionation, *J. Colloid Interface Sci.*, 2015, **457**, 131–140.
51 D. A. Urban, A. M. Milosevic, D. Bossert, F. Crippa, T. L. Moore, C. Geers, *et al.*, Taylor Dispersion of Inorganic Nanoparticles and Comparison to Dynamic Light Scattering and Transmission Electron Microscopy, *Colloid Interface Sci. Commun.*, 2018, **22**, 29–33.
52 Z. Q. Li, Z. Q. Wu and X. H. Xia, Study of Interaction of Nanoparticles and Proteins in Taylor Dispersion Analysis, *Chin. J. Anal. Chem.*, 2017, **45**(12), 1980–1987.
53 J. Chamieh and H. Cottet, Comparison of single and double detection points Taylor dispersion analysis for monodisperse and polydisperse samples, *J. Chromatogr. A*, 2012, **1241**, 123–127.
54 L. Cipelletti, J. P. Biron, M. Martin and H. Cottet, Polydispersity Analysis of Taylor Dispersion Data: The Cumulant Method, *Anal. Chem.*, 2014, **86**(13), 6471–6478.

55 H. Cottet, J. P. Biron, L. Cipelletti, R. Matmour and M. Martin, Determination of Individual Diffusion Coefficients in Evolving Binary Mixtures by Taylor Dispersion Analysis: Application to the Monitoring of Polymer Reaction, *Anal. Chem.*, 2010, **82**(5), 1793–1802.
56 H. Cottet, J. P. Biron and M. Martin, On the optimization of operating conditions for Taylor dispersion analysis of mixtures, *Analyst*, 2014, **139**(14), 3552–3562.
57 S. Latunde-Dada, R. Bott, K. Hampton, J. Patel and O. I. Leszczyszyn, Methodologies for the Taylor dispersion analysis for mixtures, aggregates and the mitigation of buffer mismatch effects, *Anal. Methods*, 2015, **7**(24), 10312–10321.
58 W. E. Price, Theory of the Taylor Dispersion Technique for 3-Component-System Diffusion Measurements, *J. Chem. Soc., Faraday Trans. 1*, 1988, **84**, 2431–2439.
59 W. Steuer, K. Jost and I. Halasz, Averaged Molecular-Weight of Complex-Mixtures as Determined by Rapid Measurements of Diffusion, *Chromatographia*, 1985, **20**(1), 13–19.
60 J. Chamieh, J. P. Biron, L. Cipelletti and H. Cottet, Monitoring Biopolymer Degradation by Taylor Dispersion Analysis, *Biomacromolecules*, 2015, **16**(12), 3945–3951.
61 J. Horvath and V. Dolnik, Polymer wall coatings for capillary electrophoresis, *Electrophoresis*, 2001, **22**(4), 644–655.
62 B. Kelly and D. G. Leaist, Using Taylor dispersion profiles to characterize polymer molecular weight distributions, *Phys. Chem. Chem. Phys.*, 2004, **6**(24), 5523–5530.
63 W. A. Boyle, R. F. Buchholz, J. A. Neal and J. L. McCarthy, Flow-Injection Analysis Estimation of Diffusion-Coefficients of Paucidisperse and Polydisperse Polymers such as Polystyrene Sulfonates, *J. Appl. Polym. Sci.*, 1991, **42**(7), 1969–1977.
64 H. Cottet, M. Martin, A. Papillaud, E. Souaid, H. Collet and A. Commeyras, Determination of dendrigraft poly-L-lysine diffusion coefficients by Taylor dispersion analysis, *Biomacromolecules*, 2007, **8**(10), 3235–3243.
65 U. Franzen and J. Østergaard, Physico-chemical characterization of liposomes and drug substance-liposome interactions in pharmaceutics using capillary electrophoresis and electrokinetic chromatography, *J. Chromatogr. A*, 2012, **1267**, 32–44.
66 H. Jensen, S. W. Larsen, C. Larsen and J. Østergaard, Physicochemical profiling of drug candidates using capillary-based techniques, *J. Drug Delivery Sci. Technol.*, 2013, **23**(4), 333–345.
67 A. Khodabandehloo and D. D. Chen, Particle sizing methods for the detection of protein aggregates in biopharmaceuticals, *Bioanalysis*, 2017, **9**(3), 313–326.
68 H. Y. Song and D. Cabooter, Relevance and Assessment of Molecular Diffusion Coefficients in Liquid Chromatography, *Chromatographia*, 2017, **80**(5), 651–663.
69 S. L. Feng, E. Shirani and D. W. Inglis, Droplets for Sampling and Transport of Chemical Signals in Biosensing: A Review, *Biosensors*, 2019, **9**(2), 14.
70 S. Y. Liu and M. Lammerhofer, Functionalized gold nanoparticles for sample preparation: a review, *Electrophoresis*, 2019, **40**(18–19), 2438–2461.
71 R. Aris, On the Dispersion of a Solute in a Fluid Flowing Through a Tube, *Proc. R. Soc. London, Ser. A*, 1956, **235**(1200), 67–77.
72 U. Sharma, N. J. Gleason and J. D. Carbeck, Diffusivity of solutes measured in glass capillaries using Taylor's analysis of dispersion and a commercial CE instrument, *Anal. Chem.*, 2005, **77**(3), 806–813.
73 C. Schaschke, Stokes-Einstein Equation, *A Dictionary of Chemical Engineering*, Oxford University Press, 2014.
74 G. Taylor, Conditions under which dispersion of a solute in a stream of solvent can be used to measure molecular diffusion, *Proc. R. Soc. London, Ser. A*, 1954, **225**(1163), 473–477.
75 S. Latunde-Dada, R. Bott, J. Crozier, M. Trikeriotis, O. I. Leszczyszyn and D. Goodall, Rapid determination of hydrodynamic radii beyond the limits of Taylor dispersion, *J. Chromatogr. A*, 2016, **1472**, 66–73.
76 J. Østergaard and H. Jensen, Simultaneous Evaluation of Ligand Binding Properties and Protein Size by Electrophoresis and Taylor Dispersion in Capillaries, *Anal. Chem.*, 2009, **81**(20), 8644–8648.
77 W. L. Hulse and R. T. Forbes, A nanolitre method to determine the hydrodynamic radius of proteins and small molecules by Taylor dispersion analysis, *Int. J. Pharm.*, 2011, **411**(1–2), 64–68.
78 F. Oukacine, A. Morel, I. Desvignes and H. Cottet, Size-based characterization of nanoparticle mixtures by the inline coupling of capillary electrophoresis to Taylor dispersion analysis, *J. Chromatogr. A*, 2015, **1426**, 220–225.
79 B. A. Williams and G. Vigh, Determination of effective mobilities and chiral separation selectivities from partially separated enantiomer peaks in a racemic mixture using pressure mediated capillary electrophoresis, *Anal. Chem.*, 1997, **69**(21), 4410–4418.
80 J. Chamieh, L. Leclercq, M. Martin, S. Slaoui, H. Jensen, J. Østergaard and H. Cottet, Limits in Size of Taylor Dispersion Analysis: Representation of the Different Hydrodynamic Regimes and Application to the Size-Characterization of Cubosomes, *Anal. Chem.*, 2017, **89**(24), 13487–13493.
81 S. Latunde-Dada, R. Bott, K. Hampton and O. I. Leszczyszyn, Analytical mitigation of solute-capillary interactions in double detection Taylor dispersion analysis, *J. Chromatogr. A*, 2015, **1408**, 255–260.
82 A. S. Parmar and M. Muschol, Hydration and Hydrodynamic Interactions of Lysozyme: Effects of Chaotropic versus Kosmotropic Ions, *Biophys. J.*, 2009, **97**(2), 590–598.
83 D. K. Wilkins, S. B. Grimshaw, V. Receveur, C. M. Dobson, J. A. Jones and L. J. Smith, Hydrodynamic radii of native and denatured proteins measured by pulse field gradient NMR techniques, *Biochemistry*, 1999, **38**(50), 16424–16431.
84 T. Wehr, R. RodriguezDiaz and C. M. Liu, Capillary electrophoresis of proteins, in *Advances in*

Chromatography, ed. P. R. Brown and E. Grushka, Marcel Dekker, New York, 1997, vol. 37, pp. 237–361.

85 E. A. S. Doherty, R. J. Meagher, M. N. Albarghouthi and A. E. Barron, Microchannel wall coatings for protein separations by capillary and chip electrophoresis, *Electrophoresis*, 2003, **24**(1–2), 34–54.

86 M. E. Pedersen, R. M. S. Haegebaert, J. Østergaard and H. Jensen, Size-based characterization of adalimumab and TNF-alpha interactions using flow induced dispersion analysis: assessment of avidity-stabilized multiple bound species, *Sci. Rep.*, 2021, **11**(1), 10.

87 J. Hong, H. M. Wu, R. K. Zhang, M. Y. He and W. Xu, The Coupling of Taylor Dispersion Analysis and Mass Spectrometry to Differentiate Protein Conformations, *Anal. Chem.*, 2020, **92**(7), 5200–5206.

88 L. Labied, P. Rocchi, T. Doussineau, J. Randon, O. Tillement, F. Lux, *et al.*, Taylor Dispersion Analysis Coupled to Inductively Coupled Plasma-Mass Spectrometry for Ultrasmall Nanoparticle Size Measurement: From Drug Product to Biological Media Studies, *Anal. Chem.*, 2021, **93**(3), 1254–1259.

89 P. Saetear, J. Chamieh, M. N. Kammer, T. J. Manuel, J. P. Biron, D. J. Bornhop, *et al.*, Taylor Dispersion Analysis of Polysaccharides Using Backscattering Interferometry, *Anal. Chem.*, 2017, **89**(12), 6710–6718.

90 P. N. Pusey and W. Vanmegen, Detection of Small Polydispersities by Photon-Correlation Spectroscopy, *J. Chem. Phys.*, 1984, **80**(8), 3513–3520.

91 T. Liu, F. Oukacine, H. Collet, A. Commeyras, L. Vial and H. Cottet, Monitoring surface functionalization of dendrigraft poly-L-lysines via click chemistry by capillary electrophoresis and Taylor dispersion analysis, *J. Chromatogr. A*, 2013, **1273**, 111–116.

92 J. Deschamps, S. G. Dutremez, B. Boury and H. Cottet, Size-Based Characterization of an Ionic Polydiacetylene by Taylor Dispersion Analysis and Capillary Electrophoresis, *Macromolecules*, 2009, **42**(7), 2679–2685.

93 T. Le Saux and H. Cottet, Size-based characterization by the coupling of capillary electrophoresis to Taylor dispersion analysis, *Anal. Chem.*, 2008, **80**(5), 1829–1832.

94 F. Oukacine, A. Geze, L. Choisnard, J. L. Putaux, J. P. Stahl and E. Peyrin, Inline Coupling of Electrokinetic Preconcentration Method to Taylor Dispersion Analysis for Size-Based Characterization of Low-UV-Absorbing Nanoparticles, *Anal. Chem.*, 2018, **90**(4), 2493–2500.

95 L. Leclercq and H. Cottet, Fast Characterization of Polyelectrolyte Complexes by Inline Coupling of Capillary Electrophoresis to Taylor Dispersion Analysis, *Anal. Chem.*, 2012, **84**(3), 1740–1743.

96 M. Y. He, P. Luo, J. Hong, X. F. Wang, H. M. Wu, R. K. Zhang, *et al.*, Structural Analysis of Biomolecules through a Combination of Mobility Capillary Electrophoresis and Mass Spectrometry, *ACS Omega*, 2019, **4**(1), 2377–2386.

97 R. K. Zhang, H. M. Wu, M. Y. He, W. J. Zhang and W. Xu, Mobility Capillary Electrophoresis-Restrained Modeling Method for Protein Structure Analysis in Mixtures, *J. Phys. Chem. B*, 2019, **123**(10), 2335–2341.

98 W. J. Zhang, H. M. Wu, R. K. Zhang, X. Fang and W. Xu, Structure and effective charge characterization of proteins by a mobility capillary electrophoresis based method, *Chem. Sci.*, 2019, **10**(33), 7779–7787.

99 H. M. Wu, R. K. Zhang, W. J. Zhang, J. Hong, Y. Xiang and W. Xu, Rapid 3-dimensional shape determination of globular proteins by mobility capillary electrophoresis and native mass spectrometry, *Chem. Sci.*, 2020, **11**(18), 4758–4765.

100 D. A. Beard and F. Wu, Apparent Diffusivity and Taylor Dispersion of Water and Solutes in Capillary Beds, *Bull. Math. Biol.*, 2009, **71**(6), 1366–1377.

101 R. Callendar and D. G. Leaist, Diffusion coefficients for binary, ternary, and polydisperse solutions from peak-width analysis of Taylor dispersion profiles, *J. Solution Chem.*, 2006, **35**(3), 353–379.

102 M. Ghanavati, H. Hassanzadeh and J. Abedi, Application of Taylor dispersion technique to measure mutual diffusion coefficient in hexane plus bitumen system, *AIChE J.*, 2014, **60**(7), 2670–2682.

103 J. P. Biron, F. Bonfils, L. Cipelletti and H. Cottet, Size-characterization of natural and synthetic polyisoprenes by Taylor dispersion analysis, *Polym. Test.*, 2018, **66**, 244–250.

104 X. Y. Jin, L. Leclercq, N. Sisavath and H. Cottet, Investigating the Influence of Phosphate Ions on Poly(L-lysine) Conformations by Taylor Dispersion Analysis, *Macromolecules*, 2014, **47**(15), 5320–5327.